IEEE Access
Multidisciplinary | Rapid Review | Open Access Journal

Received September 23, 2019, accepted October 15, 2019, date of publication October 22, 2019, date of current version November 1, 2019.

Digital Object Identifier 10.1109/ACCESS.2019.2948885

Coverage and Rate Analysis of Cache-Enabled Vertical Heterogeneous Networks

CONGSHAN FAN, TIANKUI ZHANG, (Senior Member, IEEE), AND ZHIMIN ZENG, (Member, IEEE)

School of Information and Communication Engineering, Beijing University of Posts and Telecommunications, Beijing 100876, China

Corresponding author: Tiankui Zhang (zhangtiankui@bupt.edu.cn)

This work was supported in part by the National Natural Science Foundation of China under Grant 61971060 and Grant 61502046.

ABSTRACT The unmanned aerial vehicles (UAVs) serving as the aerial base stations (ABSs) has emerged as a promising approach to improve the coverage and capacity in the 5G network. In this article, cache-enabled vertical heterogeneous network (VHetNet) is analyzed with the aid of the stochastic geometry approach. The cache-enabled VHetNet framework consisting of ABSs equipped with caches and terrestrial base station (TBSs) is proposed. In the proposed framework, the probabilistic caching strategy is adopted for ABSs and the content-centric association scheme is designed within the cache area with the cache serving radius. Based on the proposed framework, the system performance in terms of the coverage probability and the average rate are analyzed by ignoring the thermal noise under the general channel model incorporating both line-of-sight (LoS) /non-line-of-sight (NLoS) path loss and Nakagami-m fading. The theoretical analysis is verified via the Monte Carlo simulations and the impact of the network parameters on the system performance is analyzed. The simulation results show that there exits the optimal ABSs density, ABSs altitude and cache serving radius to maximize the system performance. Increasing the density of the ABSs deployed at higher altitude may decrease system performance. ABSs with higher density has the smaller optimal cache serving radius. The probabilistic caching strategy outperforms the benchmark caching strategies containing the most popular caching strategy and the random caching strategy.

INDEX TERMS Vertical heterogeneous network, UAV, cache, stochastic geometry.

I. INTRODUCTION

With the increasing of payload capacity and the decreasing of the price, the application of unmanned aerial vehicles (UAV) has expanded from the initial military field to various civil and commercial fields in recent years, such as forest fire detection, traffic control, emergency search and rescue, cargo transportation, weather monitoring and so on [1]. Among various applications, UAV-based wireless communication is regarded as a promising technology in the future cellular networks. UAVs equipped with specific wireless modules can function as the aerial base stations (ABSs) to provide reliable and cost-effective wireless communications to desired areas [2]. Compared with the traditional terrestrial base station (TBSs), ABSs have two outstanding advantages [3]. The first advantage is that ABSs can be flexibly deployed according to real-time requirements due to the mobility. For the second advantage, the ABSs located at high altitude are able to serve the terrestrial user equipments (UEs) with the line-of-sight (LoS) communication links. Moreover, the mobility of ABSs helps to adjust the position of ABSs in 3D space to avoid the obstacles between ABSs and UEs, which further increase the probability of the LoS link. Based on these advantages, ABSs can greatly improve the performance of the existing terrestrial wireless networks in terms of coverage, capacity, delay and so on. The future wireless networks will be the integration of ABSs and TBSs, forming an vertical heterogeneous network (VHetNet) [4]. A typical application scenario of VHetNet is the enhancement of the coverage and capacity in the hotspot, for example concerts or football games. In order to reap the benefits of VHetNets, massive studies have been carried out to address a number of technical challenges including channel modeling [5], [6], UAVs deployment [7], [8], trajectory optimization [9] and resource management [10]. However, the existing research focuses on the radio link between the ABSs and the ground UEs

The associate editor coordinating the review of this manuscript and approving it for publication was Zhiyong Chen.

and neglects the impact of the backhaul link. In VHetNets, the wireless backhaul link in the form of RF microwave between the ABSs and the TBSs is widely used to connect to the core network. Due to the limited backhaul capacity, heavy traffic causes severe backhaul congestion and limits the transmission rate. Referring to the BSs caching in the cellular network [11], [12], cache can also be introduced into VHetNets, forming the cache-enabled VHetNets. Contents are proactively stored in the ABSs with the fixed energy consumption and can be obtained directly from the local cache, which is greatly beneficial to wireless backhaul traffic releasing and quality of service improving [13]. However, cache-enabled VHetNets differ significantly from the cache-enabled cellular networks in terms of the channel conditions, the mobility and the energy constraints [14]. This has stimulated interest in the research on the system characterization of the cache-enabled VHetNets.

Performance analysis is an important approach to obtain an in-depth sight into cache-enabled VHetNets. The fundamental performance analysis is dedicated to character the various performance metrics in specific scenarios and investigate the effect of parameter settings on the system performance, which provides effective guidance for the actual deployment of the cache-enabled VHetNets. Stochastic geometry is an effective method to capture the randomness and the complexity of node distributions in the large-scale wireless network [15]. In stochastic geometry models, the nodes are typically distributed according to the specific point processes for different scenarios, such as UAVs network [14]–[21], cache-enabled cellular network [22]–[29] and cache-enabled UAVs network [30]–[32], enabling to characterize various system performance analytically including coverage probability, average rate, delay and so on.

A. RELATED WORK

1) PERFORMANCE ANALYSIS OF UAVs NETWORKS

The authors in [16] analyzed the coverage probability and the average achievable rate based on a more practical channel model in which LoS and non-line-of-sight (NLoS) propagation are incorporated and experience Rayleigh and Nakagami-m fading respectively. In [17], the system performance of a UAV networks, in which UAVs are intelligently positioned above user hotspots, was evaluated against cases where the UAVs are positioned in a rectangular grid or according to heuristic positioning algorithms. The research was extended to the general multi-tier drone networks in [18]. The impact of different urban environments on the optimal proportion of drones in the multitier drone network was investigated given the performance metric of spectral efficiency. Apart from the distribution model adopted by the work above in which UAVs are dispersed across the infinite space and modeled by Poisson Point Process (PPP), UAVs may be limited to the finite region in some scenarios. Modeling the finite network of UAVs as a uniform binomial point process (BPP), [19] characterized the downlink coverage probability.

The UAVs can be integrated into diversified types of networks to further improves the system performance, which give rise to a research field of new. In a drone assisted radio access networks in [20] where a given number of drones are leveraged to relay data between base stations and users, a drone deployment problem was formulated and solved to maximize the user coverage and maintain drone-to-base station link qualities. An analytical framework to analyze the signal to interference plus noise ratio (SINR) coverage probability of UAV assisted cellular networks with clustered UEs was presented in [21]. A hybrid network, in which two UAVs in post-disaster area cooperated to serve numerous vehicles on the ground for disaster response and relief was proposed in [22]. The authors of [23] analyzed the coverage and rate performance of UAV communication in the presence of underlaid D2D communication links.

2) PERFORMANCE ANALYSIS OF CACHE-ENABLED CELLULAR NETWORKS

The authors of [24] characterized the outage probability and average content delivery rate of the cache-enabled cellular networks. In [25], A relay caching mechanism for multimedia was designed to improve the energy efficiency in cellular networks. The work in [26] investigated the energy efficiency of cache-enabled cellular networks considering the limited backhaul. Under the always-on architecture and the dynamic on-off architecture, the system performance based on the probabilistic small-cell caching strategy was analyzed in terms of successful download probability in [27]. The research was extended from the single tier cellular network [24]–[27] to the multi tier HetNets [28]–[31]. The cache-based content delivery in the three-tier HetNets was proposed in [28], where BSs, relays and users cooperated to transmit contents. The outage probability and the average ergodic rate were theoretically elaborated. The work in [29] analyzed the interplay of caching and spectrum sharing under the probabilistic caching framework in the HetNets with the performance index of the outage probability. Different from the uncoded caching, the coded caching in a large-scale small-cell network was investigated in [30] and the performance was characterized by two metrics of the average fractional offloaded traffic and the average ergodic rate. To provide high spatial file diversity and ensure efficient content dissemination, [31] jointly considered the caching and the multicasting in the large-scale HetNets. However, the research methods for the cache-enabled cellular network can not be applied directly to the cache-enabled VHetNets due to the significant differences between the ABSs and TBSs, such as space deployment, channel characteristics, mobility and so on.

3) CACHE-ENABLED UAVs NETWORKS

In [32], distributed caching strategy and the interference management scheme was investigated under a proposed framework of caching UAV-enabled small cell networks. The authors of [33] analyzed the problem of joint caching and

resource allocation in the cache-enabled UAVs network in which the ground UEs are served over the LTE licensed and unlicensed bands. References [32] and [33] proposed and optimized the caching placement of the cache-enabled UAVs networks. The work in [34] investigated the probabilistic caching placement in the heterogeneous UAVs networks and obtained the optimal caching probability by maximizing the average service success probability.

B. MOTIVATION AND CONTRIBUTIONS

The existing research of the cache-enabled UAVs networks focused on the single tier homogeneous UAVs networks and neglected the multi-tier VHetNets containing both ABSs and TBSs. Meanwhile, the channel model and the association strategy were simplified to facilitate the analysis. In the practical scenarios, ABSs usually coexist with the TBSs. According to the specific association strategy, UEs are associated with the ABSs or TBSs and experience space-to-ground and ground-to-ground channels respectively. The performance analysis should be carried out for ABSs and TBSs. This paper analyzes the cache-enabled VHetNets with the aid of the stochastic geometry approach. The main contributions are summarized as follows:

- We propose a cache-enabled VHetNets framework in which ABSs equipped caches coexist with the TBSs with the sufficient backhual capacity. We adopt the probabilistic caching strategy for ABSs and design a content-centric association scheme within the cache area centered at the user with the cache serving radius.
- We analyze the system performance in terms of the coverage probability and the average rate based on the proposed network framework by ignoring the thermal noise. The general channel model incorporating both LoS / NLoS path loss and Nakagami-m fading is used.
- We verify the accuracy of theoretical analysis via Monte Carlo simulations and analyze the impact of the network parameters on the system performance. Numerical results demonstrate that 1) the optimal ABSs density, ABSs altitude and cache serving radius are achieved to maximize the system performance. Moreover, increasing the density of the ABSs deployed at higher altitude may decrease system performance. ABSs with higher density have the smaller optimal cache serving radius. 2) The probabilistic caching strategy performs better than the benchmark caching strategies containing the most popular caching strategy and the random caching strategy.

The rest of the paper is organized as follows. Section II gives the system model for cache-enabled VHetNet. In Section III, analytical expressions for the coverage probability and the average rate are derived. Numerical results are presented in Section IV, which is followed by the conclusions in Section V.

II. SYSTEM MODEL

The system model, including VHetNet model, channel model, cache model and association model, is described in this section. The symbols used therein and their descriptions are tabulated in Table 1.

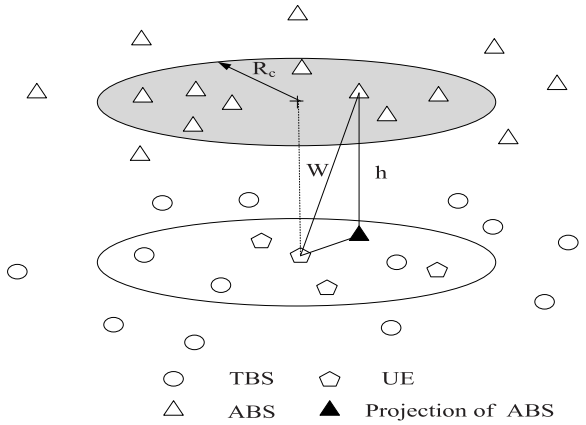

FIGURE 1. An example of cache-enabled VHetNets structure.

A. VHetNet MODEL

A two-tier cache-enabled VHetNet is considered in this paper, where a TBSs tier is overlaid with an ABSs tier consisting of UAVs. ABSs are deployed in the infinite plane at a fixed altitude of h. Denoting x_i as the location of the i th ABS, the spatial distribution of the ABSs $\Phi_A = \{x_i, i = 0, 1, 2 \ldots\}$ obeys independent PPP in the three dimensional (3-D) space and the intensity is λ_A, which effectively models the random distribution of ABSs in the wide area [35], [36]. The locations of TBSs y_j are spatially distributed according to a 2-D PPP $\Phi_T = \{y_j, j = 0, 1, 2 \ldots\}$ and the intensity is λ_T. The spatial distribution of UEs is also modeled as a 2-D PPP Φ_U. ABSs are equipped with cache and TBSs are connected to the core network via the backhaul link with sufficient capacity. According to the Palm theory, the statistical properties of UE at any position coincide with that of a typical UE at a fixed position [15]. Without loss of generality, the analysis is conducted on a typical UE at the origin, namely the tagged UE.

B. CHANNEL MODEL

The wireless channel is modeled as the combination of path loss and small scale fading. Air to ground (A2G) channel and ground to ground (G2G) channel exhibit different characteristics, the specific channel models are described as follows:

1) A2G CHANNEL MODEL

ABSs can serve UEs through LoS link or NLos link depending on the type of the UAV, elevation angle and the environment. Moreover, the path loss experienced by the NLoS link is higher than that of the LoS link due to the shadowing effect and the reflection of signals from obstacles. In view of this feature, a common approach to model the A2G channel is employed in which LoS and NLoS components are considered along with their occurrence probabilities separately [21]. Given an arbitrary ABS x_i, the occurrence probabilities of

TABLE 1. Summary of variables.

Symbol	Description
λ_A	ABSs density
λ_A	TBSs density
x_i	Location of ABS
y_j	Location of TBS
P_A	Transmission power of ABS
P_T	Transmission power of TBS
$\mathcal{P}_{LoS}$ /$\mathcal{P}_{NLoS}$	Occurrence probabilities of LoS / NLoS link
h	Altitude
φ	Elevation angle
r	Horizontal distance
ε	Link status indicator
$g_{L,i}$ / $g_{N,i}$	Channel gain of ABS for LoS / NLoS link
$h_{T,j}$	Channel gain of TBS
$\varepsilon_{L,i}$ / $\varepsilon_{N,i}$	Additional losses of ABS for LoS / NLoS link
α_L / α_N	Path-loss exponent of ABS for LoS / NLoS link
α_T	Path-loss exponent of TBS
E	Content library size
E_c	Cache capacity
γ	Content popularity shape parameter
$\mathcal{G}_n$	Content group
p_n	Caching probability
R_c	Cache serving radius of ABS
$\mathcal{B}_c$	Cache area of ABS

LoS links from x_i to the tagged UE is expressed as

$$\mathcal{P}_{LoS}(\varphi) = \frac{1}{1 + a\exp(-b(\varphi - a))}, \tag{1}$$

where a and b are constants that depend on the environment. φ denotes the elevation angle between the tagged UE and the ABS x_i and can be calculated as $\varphi = \frac{180}{\pi}\tan^{-1}\left(\frac{h}{r}\right)$, r is the Euclidean horizontal distance from x_i^* generated by the projection of the ABS x_i on the horizontal plane to the tagged UE. The occurrence probability of NLoS links is $\mathcal{P}_{NLoS}(\varphi) = 1 - \mathcal{P}_{LoS}(r)$. Since all the ABSs are deployed at the same altitude h, LoS and NLoS probabilities are functions of the horizontal distance r. For the sake of uniform description, $\mathcal{P}_{LoS}(r)$ and $\mathcal{P}_{NLoS}(r)$ hereafter are used to denote LoS and NLoS probabilities.

Based on the A2G channel model, each ABS is either in a LoS or NLoS condition with the tagged user and the LoS and NLoS transmissions are independent from each other. As a result, ABSs set can be decomposed into two independent inhomogeneous PPPs from the tagged UE's perspective $\Phi_A = \Phi_L \cup \Phi_N$, in which Φ_L and Φ_N denote the set of ABSs in LoS or NLoS conditions with the tagged UE, hereinafter referred to as LBSs and NBSs. Since the occurrence probabilities $\mathcal{P}_{LoS}(r)$ and $\mathcal{P}_{NLoS}(r)$ are functions of the horizontal distance r, the resultant PPPs are inhomogeneous. For a given altitude h, ABSs with short horizontal distances r are more likely to serve the tagged UE with the LoS link. As the altitude h increases, more ABSs are in LoS conditions with the tagged UE. For the sake of uniform description, $\varepsilon \in \{L, N\}$ is used to indicate the link status of the ABS, such as, εBS denotes the ABS in ε link with the tagged UE. In contrast, $\hat{\varepsilon}$ indicate a different link status from that of ε.

The small-scale fading of ABSs is modeled as Nakagamim fading which is universal to mimics numerous fading scenarios. Denoting $g_{L,i}$, $g_{N,i}$ as the channel gain between the tagged UE and the ABS x_i with LoS or NLoS links, $g_{L,i}, g_{N,i}$ follow Gamma distribution and the probability density functions (PDF) are given by [19]

$$f_{g_{\varepsilon,i}}(\omega) = \frac{m_\varepsilon^{m_\varepsilon}\omega^{m_\varepsilon - 1}}{\Gamma(m_\varepsilon)}\exp(-m_\varepsilon\omega), \quad \varepsilon \in \{L, N\}, \tag{2}$$

where m_L and m_N denote shape parameter for the LOS link and NLOS link respectively, $\Gamma(m_\varepsilon)$ is the Gamma function.

Let P_A denotes the transmission power, the received power at the tagged UE from ABS x_i in LoS or NLoS condition are given by

$$P_{\varepsilon,i} = P_A\eta_\varepsilon Z_{\upsilon,i}^{-\alpha_\varepsilon} g_{\varepsilon,i}, \quad \varepsilon \in \{L, N\}, \tag{3}$$

where η_L and η_N denote the mean additional losses corresponding to LoS and NLoS link, $Z_{L,i}$, $Z_{N,i}$ are the distances between the tagged UE and the ABS for NLoS and LoS link respectively α_L and α_N are the corresponding path-loss exponents.

2) G2G CHANNEL MODEL

Denoting $Z_{T,j}$ as the distance of the tagged UE from the BS y_j, the path loss is calculated with the standard power-law model as $Z_{T,j}^{-\alpha_T}$, where α_T is the path loss exponent. The small-scale fading of TBSs is modeled as the Rayleigh fading. Rayleigh fading follows the independent and identically distributed (i.i.d.) exponential distribution with mean 1, $h_{T,j} \sim \exp(1)$. Setting the transmission power of the TBSs as P_T, the received power at the tagged UE can be expressed as $P_T h_{T,j} Z_{T,j}^{-\alpha_T}$.

C. CACHE MODEL

The content library is denoted as $\mathcal{F} = \{f_1, f_2 \cdots f_{E-1}, f_E\}$ and contains $E = |\mathcal{F}|$ contents. The popularity of the content follows Zipf distribution [11]. Sorting the content in the descending order of popularity, the popularity of the e-ranked content is written as

$$s_e = \frac{e^{-\gamma}}{\sum_{i=1}^{E} i^{-\gamma}}, \tag{4}$$

where $\gamma \geq 0$ is the shape parameter, reflecting the skewness of the popularity distribution. The larger the value of γ is, the more uneven the content popularity distribution.

The cache capacity of the ABSs E_c are extremely small with respect to the enormous content library and can not afford the storage of all contents. Content library is partitioned into E/E_c non-overlapping content groups (CGs), with each CG containing E_c files. For instance, the contents in the n th CG can be shown as $\mathcal{G}_n = \{f_{E_c(n-1)+1}, f_{E_c(n-1)+2} \cdots, f_{E_c n}\}$. The probability q_n that the tagged UE requests a content in CG $\mathcal{G}_n$ is given by

$$q_n = \sum_{e=E_c(n-1)+1}^{E_c n} s_e. \tag{5}$$

Probabilistic caching strategy is carried out on the basis of CGs in which each ABS independently selects one CG to store according to the caching probability. Denote p_n as the probability that the ABS caches the n th CG, p_n satisfies

$$\sum_{n=1}^{E/E_c} p_n = 1, \tag{6}$$

$$0 \le p_n \le 1. \tag{7}$$

According to the properties of PPP, the distribution of the ABSs caching and not caching the content group $\mathcal{G}_n$ can be modeled as the thinning PPP Φ_{A,n^+}, Φ_{A,n^-}, the density are $p_n\lambda_A$, $(1-p_n)\lambda_A$. Further, Φ_{A,n^+} consists of two types of ABSs in Los links and NLos links with the tagged UE $\Phi_{A,n^+} = \Phi_{L,n^+} \cup \Phi_{N,n^+}$, the density are $\mathcal{P}_{LoS}(r)\, p_n\lambda_A$, $\mathcal{P}_{NLoS}(r)\, p_n\lambda_A$. The same classification also applies to $\Phi_{A,n^-} = \Phi_{L,n^-} \cup \Phi_{N,n^-}$.

D. ASSOCIATION STRATEGY

Define a threshold distance R_c as the cache serving radius that specifies the maximum horizontal distance over which the ABSs serve the tagged UE' content request. The finite disk $\mathcal{B}_c$ centered at the origin with radius R_c at the altitude h over the ground is referred as the cache area. The tagged UE is assumed to be associated with the ABS within $\mathcal{B}_c$ that caches the requested content and provides the maximum received power, namely the content-centric association. If no ABS caching the requested content exists within $\mathcal{B}_c$, the UE is associated with the nearest TBS and accesses the requested content from the core network via the backhaul link.

The ABSs and TBSs are assumed to operate in the same frequency spectrum. When the UE requests a content in CG $\mathcal{G}_n$ and is associated with εBS x_0, the total interference consists of all ABSs except the serving ABS and all TBSs. Since the thermal noise is very small compared to the desired signal power, it is ignored in the performance analysis [37]. The signal to interference ratio (SIR) of the UE a distance $W_{\varepsilon,n}$ from the serving εBS and has the fading g_ε is expressed as

$$SIR_{\varepsilon,n} = \frac{P_A \eta_\varepsilon g_\varepsilon W_{\varepsilon,n}^{-\alpha_\varepsilon}}{I_A + I_T}, \tag{8}$$

where I_A, I_T denote the interference from ABSs tier and TBSs tier.

Similarly, the SIR of the UE connecting to the TBS is specified as

$$SIR_{T,n} = \frac{P_T g_T W_T^{-\alpha_T}}{I_A + I_T}, \tag{9}$$

where W_T is the distance between the serving TBS y_0 and the UE, g_T is the corresponding fading. I_A, I_T denote the interference from ABSs tier and TBSs tier.

III. PERFORMANCE ANALYSIS

This section analyzes the coverage probability and the average rate of the cache-enabled VHetNet.

A. COVERAGE PROBABILITY

Coverage probability is defined as the probability that the requested content of the tagged UE is successfully accessed and the received SIR is higher than the prescribed threshold. Based on the association strategy, the tagged UE can be served by LBS, NBS and TBS when the content request is initiated. Combining with the request probability q_n and applying the law of total probability, the coverage probability is given by

$$\begin{aligned} C &= \sum\nolimits_{n=1}^{E/E_c} q_n \mathbb{P}\left(SIR_n \ge \theta\right) \\ &= \sum\nolimits_{n=1}^{E/E_c} q_n A_{L,n} \mathbb{P}\underbrace{\left(SIR_{L,n} \ge \theta\right)}_{C_{L,n}} \\ &\quad + q_n A_{N,n} \mathbb{P}\underbrace{\left(SIR_{N,n} \ge \theta\right)}_{C_{N,n}} + q_n A_{T,n} \mathbb{P}\underbrace{\left(SIR_{T,n} \ge \theta\right)}_{C_{T,n}}, \end{aligned} \tag{10}$$

where $A_{L,n}$, $A_{N,n}$ and $A_{T,n}$ denote the association probabilities that the tagged UE requests content from $\mathcal{G}_n$ and is associated with LBS, NBS or TBS, $C_{L,n}$, $C_{N,n}$ and $C_{T,n}$ are conditional coverage probabilities given the corresponding connecting status.

According to the proposed association strategy, the tagged UE is associated with the nearest TBS or the ABS that caches the requested content and provides the maximum received power. Due to the differences in path-loss exponents and the mean additional losses corresponding to LoS and NLoS link, the nearest ABS may not provide the maximum received power. For instance, a further LBS may provide larger received power than a closer NBS given the path loss parameters satisfying $\eta_L > \eta_N$ and $\alpha_L < \alpha_N$. However, the ABSs in the same link conditions with the tagged UE have the same path loss exponents and the mean additional losses. Accordingly, within the set Φ_L or Φ_N, the closest LBS or NBS provide the maximum received power. Based on the combination of the cache status and the link condition, the nearest LBS or NBS caching the requested content may be selected as the serving ABSs from the Φ_{L,n^+} or Φ_{N,n^+}. In the following, the expressions for the distribution of the distances between the tagged UE and the nearest LBS, NBS and TBS capable of accessing the requested content from the local cache or the core network are firstly derived. Based on the distance distribution, the expressions for the association probabilities and the serving distances distribution are obtained. At last, the coverage probability is characterized according to formula (10) using the auxiliary results.

Lemma 1: The probability density functions (PDF) of the Euclidean distance between the tagged UE and the closest LBS, NBS and TBS that cache the content group $\mathcal{G}_n$, denoted by $V_{L,n}$, $V_{N,n}$ and $V_{T,n}$, are

given by

$$f_{V_{L,n}}(v) = -2\pi p_n \lambda_A \mathcal{P}_L\left(\sqrt{v^2-h^2}\right) v \times \exp\left(-2\pi p_n \lambda_A \int_0^{\sqrt{v^2-h^2}} \mathcal{P}_L(r) r dr\right), \quad v \geq h, \tag{11}$$

$$f_{V_{N,n}}(v) \quad -2\pi p_n \lambda_A \mathcal{P}_N\left(\sqrt{v^2-h^2}\right) v \times \exp\left(-2\pi p_n \lambda_A \int_0^{\sqrt{v^2-h^2}} \mathcal{P}_N(r) r dr\right), \quad v \geq h, \tag{12}$$

$$f_{V_{T,n}}(v) = -2\pi \lambda_T v \exp\left(-\pi \lambda_T v^2\right), \quad v \geq 0. \tag{13}$$

Proof: Please refer to Appendix A. □

Based on **Lemma 1**, the association probabilities for LBS, NBS are derived on the premise of cache area $\mathcal{B}_C$ by jointly considering the cache status and the link condition. In contrast, the association probability for TBS is equivalent to the probability that no ABSs caching the requested content exists within $\mathcal{B}_C$. The specific association probabilities are given in the following lemmas.

Lemma 2: The probability that the tagged UE requests the content from the content group $\mathcal{G}_n$ and is associated with a specific type of BS among LBS, NBS and TBS is given by

$$A_{L,n} = \int_h^{\sqrt{R_c^2+h^2}} \exp\left(-2\pi p_n \lambda_A \int_0^{D_{LN}(v)} \mathcal{P}_N(z) z dz\right) \times f_{V_{L,n}}(v)\, dv, \tag{14}$$

$$A_{N,n} = \int_h^{\sqrt{R_c^2+h^2}} \exp\left(-2\pi p_n \lambda_A \int_0^{D_{NL}(v)} \mathcal{P}_L(z) z dz\right) \times f_{V_{N,n}}(v)\, dv, \tag{15}$$

$$A_{T,n} = \exp\left(-\pi p_n \lambda_A R_c^2\right). \tag{16}$$

where $D_{LN}(v) = \sqrt{(\max\{l_{LN}(v), h\})^2 - h^2}$, $D_{NL}(v) = \min\left\{\sqrt{l_{NL}^2(v) - h^2}, R_c\right\}$, $d_{NL}(v) = \left(\frac{\eta_L}{\eta_N}\right)^{\frac{1}{\alpha_L}} v^{\frac{\alpha_N}{\alpha_L}}$, $d_{LN}(v) = \left(\frac{\eta_N}{\eta_L}\right)^{\frac{1}{\alpha_N}} v^{\frac{\alpha_L}{\alpha_N}}$. *Given the serving εBS locating v away from the tagged UE, $D_{\varepsilon\hat{\varepsilon}}(v)$ represents the minimum horizontal Euclidean distance limit between the $\hat{\varepsilon}$BS caching the requested content and the UE.*

Proof: Please refer to Appendix B. □

The serving distance distributions are analyzed according to the connecting status of the tagged UE. For TBS, the serving distance is the nearest distance, the PDF of the serving distance is equivalent to $f_{V_{T,n}}(v)$. For ABS, the PDF of the serving distance are derived based on the association probabilities and expressed in the following lemma.

Lemma 3: Given that the tagged UE requests the content from the content group $\mathcal{G}_n$ and is associated with a LBS or NBS, the PDFs of the distance between the tagged UE and the serving LBS or NBS, denoted by $f_{W_{L,n}}(w)$, $f_{W_{N,n}}(w)$, are given by

$$f_{W_{L,n}}(w) = \frac{f_{V_{L,n}}(w)}{A_{L,n}} \exp\left(-2\pi p_n \lambda_A \int_0^{D_{LN}(w)} \mathcal{P}_N(r) r dr\right), \tag{17}$$

$$f_{W_{N,n}}(w) = \frac{f_{V_{N,n}}(w)}{A_{N,n}} \exp\left(-2\pi p_n \lambda_A \int_0^{D_{NL}(w)} \mathcal{P}_L(r) r dr\right). \tag{18}$$

where $D_{LN}(w) = \sqrt{(\max\{d_{LN}(w), h\})^2 - h^2}$, $D_{NL}(w) = \min\left\{\sqrt{d_{NL}^2(w) - h^2}, R_c\right\}$, $d_{LN}(w) = \left(\frac{\eta_N}{\eta_L}\right)^{\frac{1}{\alpha_N}} w^{\frac{\alpha_L}{\alpha_N}}$, $d_{NL}(w) = \left(\frac{\eta_L}{\eta_N}\right)^{\frac{1}{\alpha_L}} w^{\frac{\alpha_N}{\alpha_L}}$.

Proof: Please refer to Appendix C. □

With the auxiliary conclusions obtained, the conditional coverage probabilities for ABS, TBS are analyzed in sequence.

(1) Conditional Coverage Probability of ABSs

Assuming that the tagged UE requests the content from the content group $\mathcal{G}_n$ and is associated with εBS located w away from the UE, the conditional coverage probability is derived as follows

$$\begin{aligned} C_{\varepsilon,n} &= \mathbb{P}\left(SIR_{\varepsilon,n} \geq \theta\right) \\ &= \int_h^{\sqrt{R_c^2+h^2}} \mathbb{P}\left(\frac{P_A \eta_\varepsilon w^{-\alpha_\varepsilon} g_\varepsilon}{I_A + I_T} \geq \theta\right) f_{W_{\varepsilon,n}}(w)\, dw \\ &= \int_h^{\sqrt{R_c^2+h^2}} \mathbb{P}\left(g_\varepsilon \geq \theta P_A^{-1} \eta_\varepsilon^{-1} w^{\alpha_\varepsilon} (I_A + I_T)\right) f_{W_{\varepsilon,n}}(w)\, dw \\ &\overset{(a)}{=} \int_h^{\sqrt{R_c^2+h^2}} \mathbb{E}_{I_A,I_T}\left\{\sum_{k=0}^{m_\varepsilon-1} \frac{\left(m_\varepsilon \theta P_A^{-1} \eta_\varepsilon^{-1} w^{\alpha_\varepsilon} (I_A + I_T)\right)^k}{k!} \times \exp\left(-m_\varepsilon \theta P_A^{-1} \eta_\varepsilon^{-1} w^{\alpha_\varepsilon} (I_A + I_T)\right)\right\} f_{W_{\varepsilon,n}}(w)\, dw, \end{aligned} \tag{19}$$

(a) holds due to the fact that g_ε follows Gamma distribution, let $s_\varepsilon = m_\varepsilon \theta P_A^{-1} \eta_\varepsilon^{-1} w^{\alpha_\varepsilon}$,

$$\begin{aligned} C_{\varepsilon,n} &= \int_h^{\sqrt{R_c^2+h^2}} \mathbb{E}_{I_A,I_T}\left\{\sum_{k=0}^{m_\varepsilon-1} \frac{s_\varepsilon^k}{k!} (I_A + I_T)^k \exp\left(-s_\varepsilon (I_A + I_T)\right)\right\} \times f_{W_{\varepsilon,n}}(w)\, dw \\ &= \int_h^{\sqrt{R_c^2+h^2}} \mathbb{E}_{I_A,I_T}\left\{\sum_{k=0}^{m_\varepsilon-1} \frac{(-s_\varepsilon)^k}{k!} \frac{d^k}{ds_\varepsilon^k} \exp\left(-s_\varepsilon (I_A + I_T)\right)\right\} \times f_{W_{\varepsilon,n}}(w)\, dw \\ &= \int_h^{\sqrt{R_c^2+h^2}} \sum_{k=0}^{m_\varepsilon-1} \frac{(-s_\varepsilon)^k}{k!} \frac{d^k}{ds_\varepsilon^k} \left(\mathcal{L}_{I_A}(s_\varepsilon)\, \mathcal{L}_{I_T}(s_\varepsilon)\right) f_{W_{\varepsilon,n}}(w)\, dw, \end{aligned} \tag{20}$$

where $\mathcal{L}(\cdot)$ denotes the Laplace transform.

The aggregate interference from ABSs can be divided into four independent parts according to the cache status and the

link condition

$$I_A = I_{\varepsilon L,n^+} + I_{\varepsilon N,n^+} + I_{\varepsilon L,n^-} + I_{\varepsilon N,n^-}. \tag{21}$$

- $I_{\varepsilon L,n^+}$ comes from LBSs caching $\mathcal{G}_n$, which are distributed outside a disc of radius $l_{\varepsilon L}(w)$. For serving ABSs in different link conditions with the tagged UE, $l_{\varepsilon L}(w)$ is specified as $l_{LL}(w) = \sqrt{w^2 - h^2}$, $l_{NL}(w) = D_{NL}(w)$;
- $I_{\varepsilon N,n^+}$ comes from NBSs caching $\mathcal{G}_n$, which are distributed outside a disc of radius $l_{\varepsilon N}(w)$. For serving ABSs in different link conditions with the tagged UE, $l_{\varepsilon N}(v)$ is specified as $l_{LN}(w) = D_{LN}(w)$, $l_{NN}(w) = \sqrt{w^2 - h^2}$;
- $I_{\varepsilon L,n^-}$ comes from LBSs not caching $\mathcal{G}_n$, which are dispersed across the entire area;
- $I_{\varepsilon N,n^-}$ comes from NBSs not caching $\mathcal{G}_n$, which are dispersed across the entire area.

The Laplace transforms of $I_{\varepsilon L,n^+}$ is derived as follows

$$\begin{aligned}
&\mathcal{L}_{I_{\varepsilon L,n^+}}(s_\varepsilon) \\
&= \mathbb{E}_{I_{\varepsilon L,n^+}}\left[\exp\left(-s_\varepsilon I_{\varepsilon L,n^+}\right)\right] \\
&= \mathbb{E}_{\Phi_{L,n},g_{L,i}}\left(\exp\left(-s_\varepsilon \sum_{x_{L,i}\in\Phi_{L,n^+}/x_0} P_A \eta_L g_{L,i} Z_{L,i}^{-\alpha_L}\right)\right) \\
&= \mathbb{E}_{\Phi_{L,n}}\left\{\prod_{x_{L,i}\in\Phi_{L,n^+}/x_0} \mathbb{E}_{g_{L,i}}\left(\exp\left(-s_\varepsilon P_A \eta_L g_{L,i} Z_{L,i}^{-\alpha_L}\right)\right)\right\} \\
&\overset{(a)}{=} \mathbb{E}_{\Phi_{L,n}}\left\{\prod_{x_{L,i}\in\Phi_{L,n^+}/x_0} \left(\frac{m_L}{s_\varepsilon P_A \eta_L Z_{L,i}^{-\alpha_L} + m_L}\right)^{m_L}\right\} \\
&\overset{(b)}{=} \exp\Bigg(-2\pi p_n \lambda_A \mathcal{P}_L(z) \\
&\quad \times \int_{l_{\varepsilon L}(w)}^{\infty} \left(1 - \left(\frac{m_L}{s_\varepsilon P_A \eta_L \left(z^2+h^2\right)^{-\alpha_L/2} + m_L}\right)^{m_L}\right) z dz\Bigg),
\end{aligned} \tag{22}$$

(a) holds due to the fact that g_ε follows Gamma distribution, (b) follows from the probability generating function of the PPP.

The expression of $\mathcal{L}_{I_{\varepsilon N,n^+}}(s_\varepsilon)$, $\mathcal{L}_{I_{\varepsilon L,n^-}}(s_\varepsilon)$, $\mathcal{L}_{I_{\varepsilon N,n^-}}(s_\varepsilon)$ can be obtained through similar derivation as $\mathcal{L}_{I_{\varepsilon L,n^+}}(s_\varepsilon)$ and are given by (23), (24), (25), as shown at the bottom of this page.

Since four parts of the interference are independent of each other, the Laplace transform of $\mathcal{L}_{I_A}(s_\varepsilon)$ is given by

$$\mathcal{L}_{I_A}(s_\varepsilon) = \mathcal{L}_{I_{\varepsilon L,n^+}}(s_\varepsilon)\,\mathcal{L}_{I_{\varepsilon N,n^+}}(s_\varepsilon)\,\mathcal{L}_{I_{\varepsilon L,n^-}}(s_\varepsilon), \tag{26}$$

The Laplace transforms of $\mathcal{L}_{I_T}(s_\varepsilon)$ is derived as follows

$$\begin{aligned}
\mathcal{L}_{I_T}(s_\varepsilon) &= \mathbb{E}_{\Phi_T,g_j}\left(\exp\left(-s_\varepsilon \sum_{y_j\in\Phi_T} P_T g_{T,j} Z_{T,j}^{-\alpha_T}\right)\right) \\
&\overset{(a)}{=} \mathbb{E}_{\Phi_T}\left(\prod_{y_j\in\Phi_T} \frac{1}{s_\varepsilon P_T Z_{T,j}^{-\alpha_T} + 1}\right) \\
&\overset{(b)}{=} \exp\left(-2\pi\lambda_T \int_0^\infty \left(1 - \frac{1}{s_\varepsilon P_T z^{-\alpha_T} + 1}\right) z dz\right) \\
&= \frac{2\pi\lambda_T (s_\varepsilon P_T)^{2/\alpha_T}}{\alpha_T} B\left(\frac{2}{\alpha_T}, 1 - \frac{2}{\alpha_T}\right),
\end{aligned} \tag{27}$$

where $B(\cdot)$ is the Beta function, (a) follows from $g_{T,j} \sim \exp(1)$, (b) follows from the probability generating function of the PPP.

Integrating (26) and (27) into (20), the conditional coverage probability $C_{\varepsilon,n}$ is obtained.

(2) Conditional Coverage Probability of TBSs

Assuming that the tagged UE requests the content from the content group $\mathcal{G}_n$ and is associated with TBS, the conditional coverage probability is derived as follows

$$\begin{aligned}
C_{T,n} &= \mathbb{P}\left(SIR_{T,n} \geq \theta\right) \\
&= \int_0^\infty \mathbb{P}\left(\frac{P_T v^{-\alpha_T} g_T}{I_A + I_T} \geq \theta\right) f_{V_{T,n}}(v) dv \\
&= \int_0^\infty \mathbb{P}\left(g_T \geq \theta P_T^{-1} v^{\alpha_T}\left(I_A + I_T\right)\right) f_{V_{T,n}}(v) dv \\
&\overset{(a)}{=} \int_0^\infty \exp\left(\theta P_T^{-1} v^{\alpha_T}\left(I_A + I_T\right)\right) f_{V_{T,n}}(v) dv,
\end{aligned} \tag{28}$$

where equality (a) holds due to $g_T \sim \exp(1)$, let $s_T = \theta P_T^{-1} v^{\alpha_T}$,

$$\begin{aligned}
C_{T,n} &= \int_0^\infty \exp\left(s_T\left(I_A + I_T\right)\right) f_{V_{T,n}}(v) dv \\
&= \int_0^\infty \mathcal{L}_{I_A}(s_T)\,\mathcal{L}_{I_T}(s_T) f_{V_{T,n}}(v) dv.
\end{aligned} \tag{29}$$

The aggregate interference from ABSs can be divided into two independent parts according to the link condition, namely

$$\mathcal{L}_{I_{\varepsilon N,n^+}}(s_\varepsilon) = \exp\left(-2\pi p_n \lambda_A \int_{l_{\varepsilon N}(w)}^\infty \left(1 - \left(\frac{m_N}{s_\varepsilon P_A \eta_N \left(z^2+h^2\right)^{-\alpha_N/2} + m_N}\right)^{m_N}\right) \mathcal{P}_N(z)\, z dz\right), \tag{23}$$

$$\mathcal{L}_{I_{\varepsilon L,n^-}}(s_\varepsilon) = \exp\left(-2\pi\left(1 - p_n\right)\lambda_A \int_0^\infty \left(1 - \left(\frac{m_L}{s_\varepsilon P_A \eta_L \left(z^2+h^2\right)^{-\alpha_L/2} + m_L}\right)^{m_L}\right) \mathcal{P}_L(z)\, z dz\right), \tag{24}$$

$$\mathcal{L}_{I_{\varepsilon N,n^-}}(s_\varepsilon) = \exp\left(-2\pi\left(1 - p_n\right)\lambda_A \int_0^\infty \left(1 - \left(\frac{m_N}{s_\varepsilon P_A \eta_N \left(z^2+h^2\right)^{-\alpha_N/2} + m_N}\right)^{m_N}\right) \mathcal{P}_N(z)\, z dz\right) \tag{25}$$

I_{TL} and I_{TN}. I_{TL}, I_{TN} comes from LBSs or NBSs, which are dispersed across the entire area

$$I_A = I_{TL} + I_{TN}. \tag{30}$$

The derivation process of $\mathcal{L}_{I_{TL}}(s_T)$, $\mathcal{L}_{I_{TN}}(s_T)$ and $\mathcal{L}_{I_T}(s_T)$ are similar to the Laplace transforms in $C_{A,n}$

$$\begin{aligned}&\mathcal{L}_{I_{TL}}(s_T)\\&= \exp\Bigg(-2\pi\lambda_A\mathcal{P}_L(z)\\&\quad\times\int_0^\infty\left(1-\frac{1}{s_T P_A \eta_L\left(z^2+h^2\right)^{-\alpha_L/2}+1}\right)zdz\Bigg),\end{aligned} \tag{31}$$

$$\begin{aligned}&\mathcal{L}_{I_{TN}}(s_T)\\&= \exp\Bigg(-2\pi\lambda_A\mathcal{P}_N(z)\\&\quad\times\int_0^\infty\left(1-\frac{1}{s_T P_A \eta_N\left(z^2+h^2\right)^{-\alpha_N/2}+1}\right)zdz\Bigg),\end{aligned} \tag{32}$$

$$\begin{aligned}&\mathcal{L}_{I_T}(s_T)\\&= \exp\Bigg(-\frac{2\pi\lambda_D s_T P_t v^{2-\alpha_T}}{\alpha-2}\\&\quad\times {}_2F_1\left(1,\frac{\alpha-2}{\alpha};2-\frac{2}{\alpha};-s_T P_t v^{-\alpha_T}\right)\Bigg),\end{aligned} \tag{33}$$

where ${}_2F_1(\cdot)$ is the Gauss hypergeometric function. Integrating $\mathcal{L}_{I_A}(s_T) = \mathcal{L}_{I_{TL}}(s_T)\mathcal{L}_{I_{TN}}(s_T)$ and $\mathcal{L}_{I_T}(s_T)$ into (29), the conditional coverage probability $C_{T,n}$ is obtained.

B. AVERAGE RATE

The average rate is defined as the average delivery rate achievable by the tagged UE when the requested content is successfully accessed. With the Shannon capacity formula $R = \mathbb{E}(log_2(1+SIR))$, the average rate is analyzed and given in the following theorem.

Lemma 4: The ergodic rate achievable by a tagged UE in a two-tier VHetNet is given by (34)*, as shown at the bottom of this page.*

Proof: Similar to the coverage probability, average rate is analysed separately for the specific connecting status. Given that the tagged UE requests content from $\mathcal{G}_n$ and is associated with LBS, the achievable instantaneous rate, denoted by the random variable $R_{L,n}$ is calculated by $R_{L,n} = log_2(1+SIR_{L,n})$, its expected value can be evaluated as

$$\begin{aligned}\bar{R}_{L,n} &= \mathbb{E}(R_{L,n})\\&\overset{(a)}{=}\int_0^\infty \mathbb{P}(R_{L,n}\geq\tau)d\tau\\&=\int_0^\infty\int_h^\infty \mathbb{P}\left(log_2\left(1+SIR_{L,n}(w)\right)\geq\tau\right)f_{W_{L,n}}(w)dwd\tau\\&=\int_0^\infty\int_h^\infty \mathbb{P}\left(SIR_{L,n}(w)\geq 2^\tau-1\right)f_{W_{L,n}}(w)dwd\tau,\end{aligned} \tag{35}$$

where (a) follows from the fact that $\mathbb{E}(X)=\int_0^\infty(X\geq\gamma)\,d\gamma$ holds for a positive random variable X. The following proof is the same as $C_{L,n}$ by assuming $s_L = m_L(2^\tau-1)P_A^{-1}\eta_L^{-1}w^{\alpha_L}$.

The derivation process of $\bar{R}_{N,n}$, $\bar{R}_{T,n}$ are similar to $\bar{R}_{L,n}$. □

IV. NUMERICAL RESULT

In this section, both the numerical simulations and Monte Carlo simulations are presented. The scenario of the two-tier VHetNets is considered, in which ABSs and TBSs are distributed according to PPP in a circular area with 200 km radius. We assume that the ABS is operating in an urban environment with the parameters shown in Table 2. The results are averaged over 10000 Monte Carlo trials. The optimal caching probability is obtained by maximizing the coverage probability or the average rate with the genetic algorithm, as shown in Algorithm 1. The procedure of the genetic algorithm for maximizing the average rate is similar. We validate the theoretical analysis in the previous section via Monte Carlo simulations. The impact of various parameters on the system performance are investigated.

The performance of the coverage probability with respect to different system parameters including SIR threshold, ABSs altitude, ABSs density, cache radius, ABSs cache capacity and content popularity distribution parameter are shown in Fig. 2- Fig. 6. It can be seen from the figures that the simulation curves match with the numerical curves, which gives an effective validation of the theoretical analysis.

$$\begin{aligned}\bar{R} &= \textstyle\sum_{n=1}^{E/E_c} q_n\left(A_{L,n}\bar{R}_{L,n}+A_{N,n}\bar{R}_{N,n}+A_{T,n}\bar{R}_{T,n}\right),\\\bar{R}_{L,n} &= \int_0^\infty\int_h^{\sqrt{R_c^2+h^2}}\sum_{k=0}^{m_L-1}\frac{(-s_L)^k}{k!}\frac{d^k}{ds_L^k}\left(\mathcal{L}_{I_A}(s_L)\mathcal{L}_{I_T}(s_L)\right)f_{W_{L,n}}(w)\,dwd\tau\Big|_{s_L=m_L(2^\tau-1)P_A^{-1}\eta_L^{-1}w^{\alpha_L}},\\\bar{R}_{N,n} &= \int_0^\infty\int_h^{\sqrt{R_c^2+h^2}}\sum_{k=0}^{m_N-1}\frac{(-s_N)^k}{k!}\frac{d^k}{ds_N^k}\left(\mathcal{L}_{I_A}(s_N)\mathcal{L}_{I_T}(s_N)\right)f_{W_{N,n}}(w)\,dwd\tau\Big|_{s_N=m_N(2^\tau-1)P_A^{-1}\eta_N^{-1}w^{\alpha_N}},\\\bar{R}_{T,n} &= \int_0^\infty\int_0^\infty\mathcal{L}_{I_A}(s_T)\mathcal{L}_{I_T}(s_T)f_{V_{T,n}}(v)dvd\tau\Big|_{s_T=(2^\tau-1)P_T^{-1}v^{\alpha_T}}\end{aligned} \tag{34}$$

Algorithm 1 Genetic Algorithm

Input: N, λ_A, λ_T, P_A, P_T
Output: C

```
Setting restrictions (6): nvars, LB, UB
Setting restrictions (7):
ConstraintFunction = @constraint
Setting formula C (10):
ObjectiveFunction = @fitness
Setting options:
options =optimoptions(@fmincon,'Algorithm','sqp')
Using GA:
Setting options:
[q, fval] =
ga(ObjectiveFunction, nvars, [ ], [ ], [ ], [ ],
LB, UB, ...ConstraintFunction, options)
C = −fval
```

TABLE 2. Simulation parameters.

Parameter	Value
ABSs density [38]	$\lambda_A = 10 \times 10^{-6} m^{-2}$
TBSs density [38]	$\lambda_T = 6 \times 10^{-6} m^{-2}$
Altitude [23]	$h = 200m$
Bandwidth [23]	$W = 10MHz$
Transmit power [38]	$P_A = 32dBm, P_T = 40dBm$
SIR threshold [38]	$\theta = -10dB$
Path loss exponent [39]	$\alpha_L = 2, \alpha_N = 3, \alpha_T = 3$
Excess path loss [39]	$\eta_L = 0.7943, \eta_N = 0.01$
Environment dependent constants [39]	$a = 9.6, b = 0.28$
Shape parameter [39]	$m_L = 3, m_N = 2$
Content catalog [32]	$E = 1200$
Cache capacity [32]	$E_c = 240$

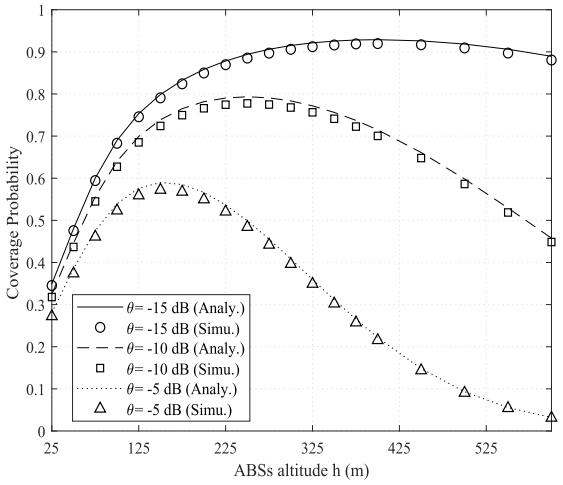

FIGURE 2. Coverage probability versus ABSs altitude with different SIR threshold, $\lambda_A = 1 \times 10^{-5}$ m^{-2}, $\gamma = 0.8$, $R_c = 600$ m.

Fig. 2 shows the evolution of the coverage probability with regard to the ABSs altitude for different SIR thresholds. It can be seen from Fig. 2 that the shape of the curves for different SIR thresholds are similar. As ABSs altitude increases, the coverage probability emerges firstly increase and then decrease trend. There exists the optimal altitude to achieve

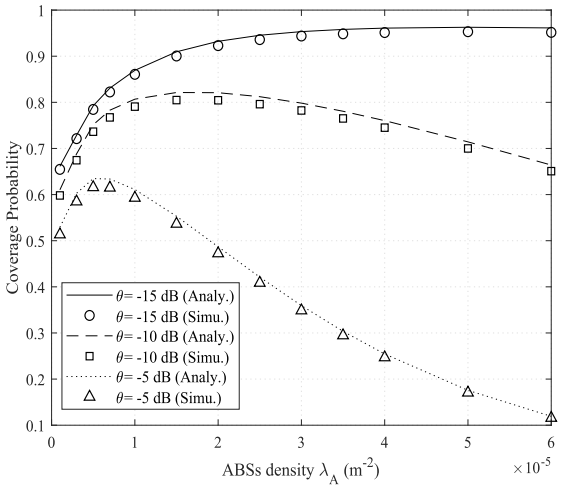

FIGURE 3. Coverage probability versus ABSs density with different SIR threshold, $h = 200$ m, $\gamma = 0.8$, $R_c = 600$ m.

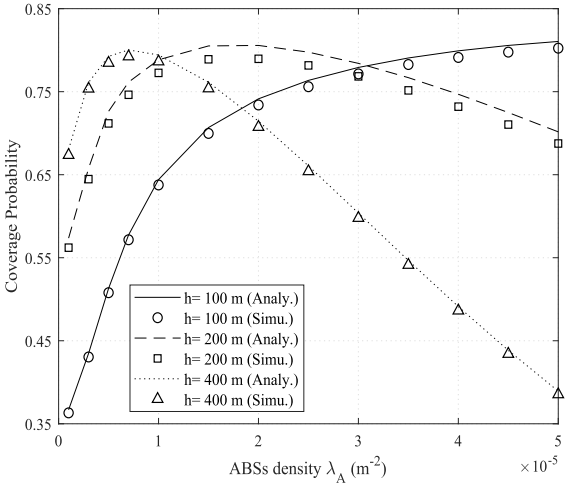

FIGURE 4. Coverage probability versus ABSs density with different ABSs altitude, $\gamma = 0.8$, $R_c = 600$ m, $\theta = -10$ dB.

the maximum coverage probability for a given SIR threshold. For ABSs deployed at low altitude, A2G channels mostly experience NLoS conditions and suffer large path-losses due to the scattering caused by the urban environment. As ABSs altitude increases, more ABSs are in LoS conditions with the UEs. The probability that the tagged UE is associated with a LBS increases. Compared with the NLoS links, LoS links have better channel conditions and increase the desired signal power, which improves the coverage probability subsequently. As the altitude continues to increase, the requested content is almost certain to be delivered through the LoS link. The coverage probability decreases due to the extended serving distance and the strong interference dominated by the LBSs. The optimal ABSs altitude to maximize the coverage probability depends on the SIR threshold. For SIR threshold setting as −15 dB, −10 dB, −5 dB, the optimal altitude is 370 m, 245 m, 155 m respectively.

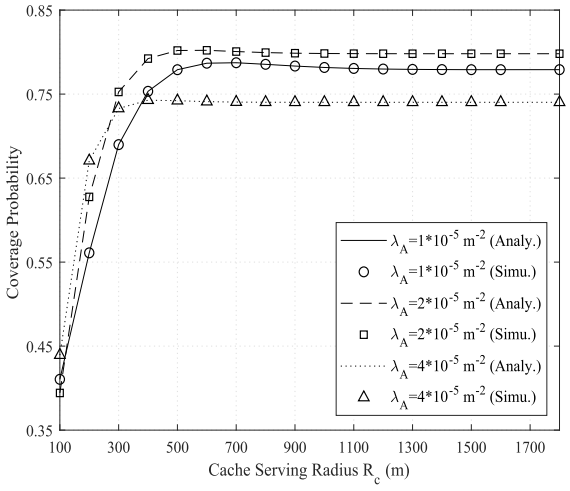

FIGURE 5. Coverage probability versus cache serving radius with different ABSs density, $h = 200$ m, $\gamma = 0.8$, $\theta = -10$ dB.

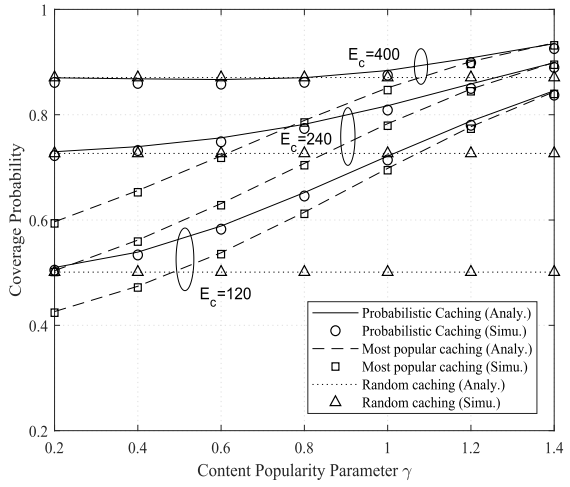

FIGURE 6. Coverage probability versus content popularity distribution parameter with different cache capacity, $h = 200$ m, $\lambda_A = 1 \times 10^{-5}$ m^{-2}, $\theta = -10$ dB, $R_c = 600$ m.

Fig. 3 depicts the impact of the ABSs density on the coverage probability for different SIR thresholds. As ABSs density increases, the coverage probability first increases and then decreases. For a given SIR threshold, there is an ABSs density at which the coverage probability is maximized. As ABSs density increases, the probability that the tagged UE is associated with an ABS increases due to the increment of the number of ABSs storing the requested content in the cache area. Moreover, dense deployment of the ABSs increases the probability of serving the tagged user with a LBS and shortens the serving distance. The coverage probability is effectively improved. With a further increase in the ABSs density, aggregate interference of ABSs increases sharply, leading to the decrease of the coverage probability. The optimal density is 4×10^{-5} m^{-2}, 1.5×10^{-5} m^{-2}, 0.4×10^{-5} m^{-2} for SIR threshold of -15 dB, -10 dB and -5 dB.

In Fig. 4, the variation of the coverage probability with regard to ABSs density for different ABSs altitude is illustrated. For low altitudes, e.g., h = 100 m, the coverage probability increases with the increment of the ABSs density and then decreases. when ABSs are deployed at low altitude, most of the ABSs experience NLoS conditions with the tagged UE, the increment of the ABSs density helps to increase the probability of accessing LBS to obtain the requested content, which increases the received signal power substantially and improves the coverage probability. As the further increment of the ABSs density, the coverage probability decrease on account of the increasing interference power dominated by NBSs and TBSs. For high altitudes, e.g., h = 400 m, the coverage probability experience slight increase initially and then severe decrease. when ABSs are deployed at high altitude, most of the ABSs experience LoS conditions with the tagged user, the tagged UE almost certainly accesses LBS to obtain the requested content. The increment of the ABSs density has less effect on the received signal power, but causes the increasing interference power dominated by LBSs.

Fig. 5 depicts the impact of the cache serving radius on the coverage probability for different ABSs density. As cache serving radius increases initially, the probability that the tagged UE is associated with the ABS increases for the case that the tagged UE requests content with high popularity. Los transmission can increases the received signal power and improves the coverage probability. As the cache serving radius continues to increase 700 m $< R_c <$ 1100 m, the tagged UE associates with the ABS as well when requesting the content with low popularity. However, the distance between the tagged UE and the serving ABS increases, the coverage probability decreases slightly. The smaller the density of ABSs, the greater the decrease. As R_c increases from 700 m to 1100 m for $\lambda_A = 1 * 10^{-5} m^{-2}$, the coverage probability decreases from 0.7880 to 0.7790. When $R_c >$1100 m, the tagged UE is certain to associate with the ABS. Increasing the cache serving radius has no effect on the link condition between the tagged UE and the serving ABS. Coverage probability no longer changes. For small cache serving radiuses, e.g., $R_c <$300 m, increasing the ABSs density can increase the probability of UEs' accessing to ABSs for content delivery and improve the coverage probability. For large cache serving radiuses, e.g., $R_c >$500 m, the tagged UE is certain to access to ABSs for content delivery. Increasing the ABSs density will cause sharp increment of the ABSs interference and decrease the coverage probability.

Fig. 6 depicts the impact of the content popularity distribution parameter γ on the coverage probability for different ABSs capacity. The proposed caching strategy is compared with two common caching policies, namely the most popular caching policy in which contents are stored in the ABSs in order of the content popularity until the cache capacity is exhausted and the random caching policy in which contents are randomly selected to store regardless of the content popularity. Given the fixed ABSs cache capacity, the coverage probability increases with the increasing γ. As γ increases, the content popularity distribution become more skewed. A high number of content requests from users

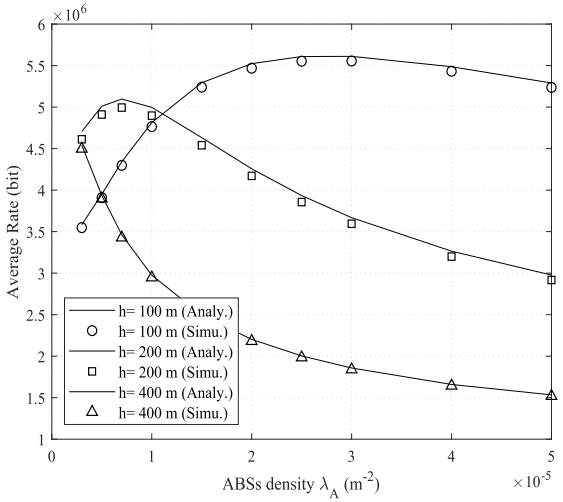

FIGURE 7. Average rate versus ABSs density with different ABSs altitude, $\gamma = 0.8$, $R_c = 600$ *m*.

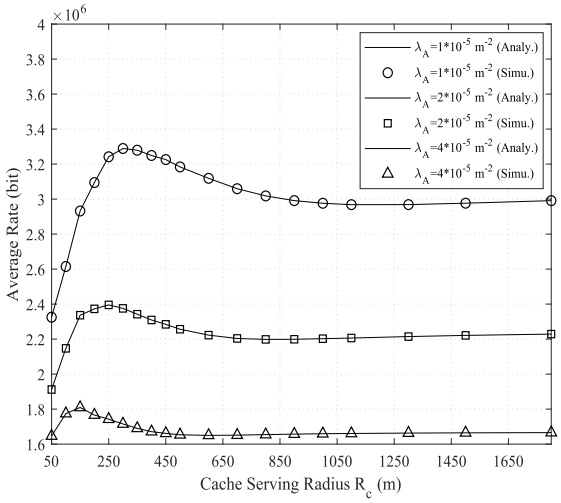

FIGURE 8. Average rate versus cache radius with different ABSs density, $h = 200$ *m*, $\gamma = 0.8$.

focus on the popular contents belonging to the top-ranking content groups and can be satisfied by most ABSs due to the high caching ratio. The coverage probability improves accordingly. The increment of the ABSs cache capacity helps to improve the coverage probability owing to high cache hit ratio. Probabilistic caching policy outperforms the most popular caching policy and the random caching strategy. Probabilistic caching strategy can improve the cache hit ratio by increasing the diversity of cached contents on the one hand and satisfy the SIR requirement by ensuring the link condition on the other hand, which results in better coverage probability performance compared with two common caching policies. For a small γ indicating more even content popularity distribution, the probabilistic caching strategy is able to cope with the diversity of content, whose performance is similar to that of the random caching strategy. For a big γ indicating more uneven content popularity distribution, the probabilistic caching strategy can improve the cache hit ratio, whose performance is similar to that of the most popular caching policy.

The performance of the average rate with respect to different system parameters including ABSs altitude, ABSs density, cache radius, ABSs cache capacity and content popularity distribution parameter are shown in Fig. 7- Fig. 9. It can be seen from the figures that the simulation curves are in agreement with the numerical curves.

The variations of the average rate with regard to ABSs density for different ABSs height are illustrated in Fig. 7. For ABSs hovering at the low altitude, as the ABSs density increases, the average rate first increases benefitting from the increment of the probability of the LoS link in the ABSs tier, then decreases on account of the large interference power. For ABSs hovering at the high altitude, the serving ABS already adopts the LoS transmission with large probability. The average rate experiences a severe decline under the influence of increasing interference power from ABSs.

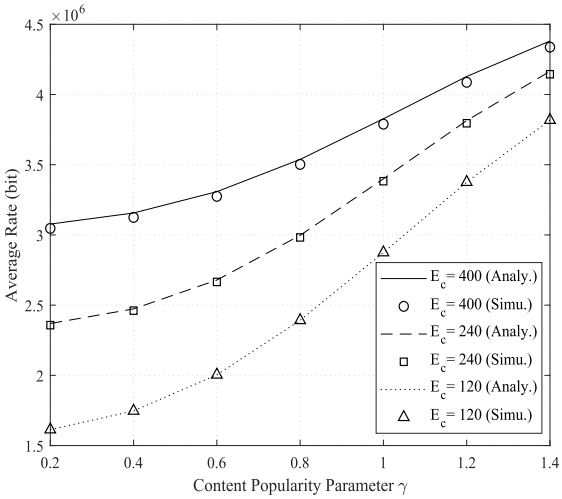

FIGURE 9. Average rate versus content popularity distribution parameter with different cache capacity, $h = 200$ m, $\lambda_A = 1 \times 10^{-5}$ m^{-2}, $R_c = 600$ m.

The variations of the average rate with regard to cache serving radius for different ABSs density are illustrated in Fig. 8. The shape of the curves for different ABSs density are consistent. The average rate increases with the increasing cache serving radius and then decreases. The reason lies in that the association probability of the ABSs increases with the increment of the cache serving radius and the requested content may be delivered through the Los link. As the cache serving radius continues to increase, the distance between the tagged UE and the serving ABSs increases sharply when the tagged UE requests the content with low popularity and associates with the ABS, the average rate decreases accordingly. When R_c increases beyond 1250 m, the increment of R_c hardly affects the association status of the tagged UE, the average rate no longer changes.

The variations of the average rate with regard to the content popularity distribution parameter for different ABSs

cache capacity are illustrated in Fig. 9. As γ increases, a large number of UEs tend to request the most popular contents cached in numerous ABS, the LoS transmission of the requested content can obtain the large delivery rate. Moreover, the increment of the ABSs capacity increase the hit ratio, which leads to dramatic improvements in the average rate.

V. CONCLUSION

The cache-enabled VHetNets consisting of ABSs equipped with cache and TBSs was analyzed using the stochastic geometry. The probabilistic caching strategy and the corresponding content-centric association scheme within the cache space limitation were proposed. Analytical expressions of the coverage probability and the average rate were derived under the general channel model incorporating both LoS/ NLoS path loss and Nakagami-m fading. Numerical simulations analyzed the impact of various parameters such as ABSs density, ABSs altitude, cache radius and cache capacity on the system performance and provided effective guidance for the actual deployment.

APPENDIX A

The cumulative distribution function (CDF) of $V_{L,n}$ is given by

$$\begin{aligned} F_{V_{L,n}}(v) &= \mathbb{P}\left(V_{L,n} \le v\right) = 1 - \mathbb{P}\left(\sqrt{R_{L,n}^2 + h^2} > v\right) \\ &= 1 - \mathbb{P}\left(R_{L,n} > \sqrt{v^2 - h^2}\right) \\ &\overset{(1)}{=} 1 - \exp\left(-2\pi p_n \lambda_A \int_0^{\sqrt{v^2-h^2}} \mathcal{P}_L(r) r dr\right), \end{aligned} \tag{A.1}$$

where $R_{L,n}$ is the horizontal Euclidean distance corresponding to the Euclidean distance $V_{L,n}$, (1) holds due to the null probability of the PPP. Taking the derivative of $F_{V_{L,n}}(v)$ with respect to v, $f_{V_{L,n}}(v)$ is obtained. The proof process of (12), (13) are similar to (11).

APPENDIX B

Assuming the tagged UE requests content from $\mathcal{G}_n$, the closest LBS x_0 caching $\mathcal{G}_n$ being the serving ABS should satisfy two conditions:

1. x_0 locates within the cache area $\mathcal{B}_c$.

2.UE receives larger power from x_0 than that of the closest NBS caching $\mathcal{G}_n$.

$A_{L,n}$ is equal to the probability of two conditions being satisfied [38] and can be derived as

$$\begin{aligned} &A_{L,n} \\ &= \mathbb{P}\left(h \le V_{L,n} \le \sqrt{R_c^2 + h^2} \cap P_A \eta_L V_{L,n}^{-\alpha_L} \ge P_A \eta_N V_{N,n}^{-\alpha_N}\right) \\ &= \int_h^{\sqrt{R_c^2+h^2}} \mathbb{P}\left(V_{N,n} \ge \left(\frac{\eta_N}{\eta_L}\right)^{\frac{1}{\alpha_N}} v^{\frac{\alpha_L}{\alpha_N}}\right) f_{V_{L,n}}(v) dv \end{aligned} \tag{B.1}$$

Let $d_{LN}(v) = \left(\frac{\eta_N}{\eta_L}\right)^{\frac{1}{\alpha_N}} v^{\frac{\alpha_L}{\alpha_N}}$,

$$A_{L,n} = \int_h^{\sqrt{R_c^2+h^2}} \mathbb{P}\left(\sqrt{R_{N,n}^2 + h^2} \ge d_{LN}(v)\right) f_{V_{L,n}}(v) dv \tag{B.2}$$

$R_{N,n}$ is the horizontal Euclidean distance corresponding to the Euclidean distance $V_{N,n}$. Since the altitude of the ABS is fixed, $d_{LN}(v)$ should satisfy $d_{LN}(v) \ge h$,

$$A_{L,n} = \int_h^{\sqrt{R_c^2+h^2}} \mathbb{P}\left(R_{N,n} \ge \sqrt{(\max(d_{LN}(v), h))^2 - h^2}\right) \times f_{V_{L,n}}(v) dv \tag{B.3}$$

Let $D_{LN}(v) = \sqrt{(\max\{d_{LN}(v), h\})^2 - h^2}$ denote the minimum horizontal Euclidean distance limit, NBSs caching $\mathcal{G}_n$ are limited to be distributed outside a disc of radius $D_{LN}(v)$. Using the null probability of PPP Φ_{N,n^+}, $A_{L,n}$ is obtained as

$$A_{L,n} = \int_h^{\sqrt{R_c^2+h^2}} \exp\left(-2\pi p_n \lambda_A \int_0^{D_{LN}(v)} \mathcal{P}_N(z) z dz\right) \times f_{V_{L,n}}(v) dv \tag{B.4}$$

The derivation process of $A_{N,n}$ is similar to that of $A_{L,n}$. According to the association strategy, the serving ABS is

$$\begin{aligned} &F_{W_{L,n}}(w) \\ &= \mathbb{P}\left(V_{L,n} \le w | h \le V_{L,n} \le \sqrt{R_c^2 + h^2} \cap P_A \eta_L V_{L,n}^{-\alpha_L} \ge P_A \eta_N V_{N,n}^{-\alpha_N}\right) \\ &= \frac{\mathbb{P}\left(V_{L,n} \le w \cap h \le V_{L,n} \le \sqrt{R_c^2 + h^2} \cap P_A \eta_L V_{L,n}^{-\alpha_L} \ge P_A \eta_N V_{N,n}^{-\alpha_N}\right)}{\mathbb{P}\left(h \le V_{L,n} \le \sqrt{R_c^2 + h^2} \cap P_A \eta_L V_{L,n}^{-\alpha_L} \ge P_A \eta_N V_{N,n}^{-\alpha_N}\right)} \\ &= \frac{\mathbb{P}\left(h \le V_{L,n} \le w \cap P_A \eta_L V_{L,n}^{-\alpha_L} \ge P_A \eta_N V_{N,n}^{-\alpha_N}\right)}{A_{L,n}} \\ &= \frac{1}{A_{L,n}} \int_h^w \exp\left(-2\pi p_n \lambda_A \int_0^{D_{LN}(v)} \mathcal{P}_N(z) z dz\right) f_{V_{L,n}}(v) dv \end{aligned} \tag{C.1}$$

required to be located within the cache area. Let $D_{NL}(v) = \min\left\{\sqrt{d_{NL}^2(v) - h^2}, R_c\right\}$ denote the minimum horizontal Euclidean distance limit, LBSs caching $\mathcal{G}_n$ are limited to be distributed outside a disc of radius $D_{NL}(v)$.

The association probabilities A_T is derived as follows

$$\begin{aligned} A_{T,n} &= \mathbb{P}\left(\textit{No ABSs caching } \mathcal{G}_n \textit{ exists in } \mathcal{B}_c\right) \\ &= \exp\left(-\pi p_n \lambda_A R_c^2\right) \end{aligned} \tag{B.5}$$

APPENDIX C

The distribution of $W_{L,n}$ is the distribution of $V_{L,n}$ given that the tagged UE requests the content from the content group $\mathcal{G}_n$ and is associated with a LBS. The CDF of W_L is derived as follows (C.1), as shown at the bottom of the previous page.

Taking the derivative of $F_{W_{L,n}}(w)$ with respect to w, $f_{W_{L,n}}(w)$ is obtained. The proof process of (18) is similar to (17).

REFERENCES

[1] Y. Zeng, R. Zhang, and T. J. Lim, "Wireless communications with unmanned aerial vehicles: Opportunities and challenges," *IEEE Commun. Mag.*, vol. 54, no. 5, pp. 36–42, May 2016.

[2] N. H. Motlagh, T. Taleb, and O. Arouk, "Low-altitude unmanned aerial vehicles-based Internet of Things services: Comprehensive survey and future perspectives," *IEEE Internet Things J.*, vol. 3, no. 6, pp. 899–922, Dec. 2016.

[3] M. Mozaffari, W. Saad, M. Bennis, Y.-H. Nam, and M. Debbah, "A tutorial on UAVs for wireless networks: Applications, challenges, and open problems," *IEEE Commun. Surveys Tuts.*, vol. 21, no. 3, pp. 2334–2360, 3rd Quart., 2019.

[4] M. Alzenad and H. Yanikomeroglu. (2018). *Coverage and Rate Analysis for Vertical Heterogeneous Networks (vhetnets)*. [Online]. Available: https://www.researchgate.net

[5] R. Amorim, H. Nguyen, P. Mogensen, I. Z. Kovács, J. Wigard, and T. B. Sørensen, "Radio channel modeling for UAV communication over cellular networks," *IEEE Wireless Commun. Lett.*, vol. 6, no. 4, pp. 514–517, Aug. 2017.

[6] A. Al-Hourani, S. Kandeepan, and A. Jamalipour, "Modeling air-to-ground path loss for low altitude platforms in urban environments," in *Proc. IEEE GLOBECOM*, Austin, TX, USA, Dec. 2014, pp. 2898–2904.

[7] A. Al-Hourani, S. Kandeepan, and S. Lardner, "Optimal LAP altitude for maximum coverage," *IEEE Wireless Commun. Lett.*, vol. 3, no. 6, pp. 569–572, Dec. 2014.

[8] M. Mozaffari, W. Saad, M. Bennis, and M. Debbah, "Efficient deployment of multiple unmanned aerial vehicles for optimal wireless coverage," *IEEE Commun. Lett.*, vol. 20, no. 8, pp. 1647–1650, Aug. 2016.

[9] Q. Wu, Y. Zeng, and R. Zhang, "Joint trajectory and communication design for multi-UAV enabled wireless networks," *IEEE Trans. Wireless Commun.*, vol. 17, no. 3, pp. 2109–2121, Mar. 2018.

[10] E. T. Ceran, T. Erkilic, E. Uysal-Biyikoglu, T. Girici, and K. Leblebicioglu, "Optimal energy allocation policies for a high altitude flying wireless access point," *Trans. Emerg. Telecommun. Technol.*, vol. 28, no. 4, p. e3034, 2017.

[11] L. Wang, K.-K. Wong, S. Jin, G. Zheng, and R. W. Heath, Jr., "A new look at physical layer security, caching, and wireless energy harvesting for heterogeneous ultra-dense networks," *IEEE Commun. Mag.*, vol. 56, no. 6, pp. 49–55, Jun. 2018.

[12] D. Liu and C. Yang, "Energy efficiency of downlink networks with caching at base stations," *IEEE J. Sel. Areas Commun.*, vol. 34, no. 4, pp. 907–922, Apr. 2016.

[13] D. Liu and C. Yang, "Caching at base stations with heterogeneous user demands and spatial locality," *IEEE Trans. Commun.*, vol. 67, no. 2, pp. 1554–1569, Feb. 2019.

[14] I. Bor-Yaliniz and H. Yanikomeroglu, "The new frontier in RAN heterogeneity: Multi-tier drone-cells," *IEEE Commun. Mag.*, vol. 54, no. 11, pp. 48–55, Nov. 2016.

[15] S. N. Chiu, D. Stoyan, W. S. Kendall, and J. Mecke, *Stochastic Geometry and Its Applications*. Hoboken, NJ, USA: Wiley, 2013.

[16] M. Alzenad and H. Yanikomeroglu, "Coverage and rate analysis for unmanned aerial vehicle base stations with LoS/NLoS propagation," in *Proc. IEEE GlOBECOM Workshops*, Abu Dhabi, United Arab Emirates, Dec. 2018, pp. 1–7.

[17] B. Galkin, J. Kibiłda, and L. A. Da Silva, "A stochastic model for UAV networks positioned above demand hotspots in urban environments," *IEEE Trans. Veh. Technol.*, vol. 68, no. 7, pp. 6985–6996, Jul. 2019.

[18] S. Sekander, H. Tabassum, and E. Hossain, "Multi-tier drone architecture for 5G/B5G cellular networks: Challenges, trends, and prospects," *IEEE Commun. Mag.*, vol. 56, no. 3, pp. 96–103, Mar. 2018.

[19] V. V. Chetlur and H. S. Dhillon, "Downlink coverage analysis for a finite 3-D wireless network of unmanned aerial vehicles," *IEEE Trans. Commun.*, vol. 65, no. 10, pp. 4543–4558, Jul. 2017.

[20] W. Shi, J. Li, W. Xu, H. Zhou, N. Zhang, S. Zhang, and X. Shen, "Multiple drone-cell deployment analyses and optimization in drone assisted radio access networks," *IEEE Access*, vol. 6, pp. 12518–12529, 2018.

[21] E. Turgut and M. C. Gursoy, "Downlink analysis in unmanned aerial vehicle (UAV) assisted cellular networks with clustered users," *IEEE Access*, vol. 6, pp. 36313–36324, 2018.

[22] S. Zhang and J. Liu, "Analysis and optimization of multiple unmanned aerial vehicle-assisted communications in post-disaster areas," *IEEE Trans. Veh. Technol.*, vol. 67, no. 12, pp. 12049–12060, Dec. 2018.

[23] M. Mozaffari, W. Saad, M. Bennis, and M. Debbah, "Unmanned aerial vehicle with underlaid device-to-device communications: Performance and tradeoffs," *IEEE Trans. Wireless Commun.*, vol. 15, no. 6, pp. 3949–3963, Jun. 2016.

[24] E. Baştuğ, M. Bennis, and M. Debbah, "Cache-enabled small cell networks: Modeling and tradeoffs," in *Pro. Int. Symp. Wireless Commun. Syst. (ISWCS)*, Barcelona, Spain, Aug. 2014, pp. 649–653.

[25] X. Wang, Y. Bao, X. Liu, and Z. Niu, "On the design of relay caching in cellular networks for energy efficiency," in *Proc. IEEE INFOCOM Workshops*, Shanghai, China, Apr. 2011, pp. 259–264.

[26] C. Fan, T. Zhang, Z. Zeng, and Y. Chen, "Energy efficiency analysis of cache-enabled cellular networks with limited backhaul," *Wireless Commun. Mobile Comput.*, vol. 2018, Feb. 2018, Art. no. 6910876.

[27] Y. Chen, M. Ding, J. Li, Z. Lin, G. Mao, and L. Hanzo, "Probabilistic small-cell caching: Performance analysis and optimization," *IEEE Trans. Veh. Technol.*, vol. 66, no. 5, pp. 4341–4354, May 2017.

[28] C. Yang, Y. Yao, Z. Chen, and B. Xia, "Analysis on cache-enabled wireless heterogeneous networks," *IEEE Trans. Wireless Commun.*, vol. 15, no. 1, pp. 131–145, Jan. 2016.

[29] S. Tamoor-ul-Hassan, M. Bennis, P. H. J. Nardelli, and M. Latva-Aho, "Caching in wireless small cell networks: A storage-bandwidth tradeoff," *IEEE Commun. Lett.*, vol. 20, no. 6, pp. 1175–1178, Jun. 2016.

[30] Z. Chen, J. Lee, T. Q. S. Quek, and M. Kountouris, "Cooperative caching and transmission design in cluster-centric small cell networks," *IEEE Trans. Wireless Commun.*, vol. 16, no. 5, pp. 3401–3415, May 2017.

[31] Y. Cui and D. Jiang, "Analysis and optimization of caching and multicasting in large-scale cache-enabled heterogeneous wireless networks," *IEEE Trans. Wireless Commun.*, vol. 16, no. 1, pp. 250–264, Jan. 2017.

[32] N. Zhao, F. R. Yu, L. Fan, Y. Chen, J. Tang, A. Nallanathan, and V. C. M. Leung, "Caching unmanned aerial vehicle-enabled small-cell networks: Employing energy-efficient methods that store and retrieve popular content," *IEEE Veh. Technol. Mag.*, vol. 14, no. 1, pp. 71–79, Mar. 2019.

[33] M. Chen, W. Saad, and C. Yin, "Liquid state machine learning for resource and cache management in LTE-U unmanned aerial vehicle (UAV) networks," *IEEE Trans. Wireless Commun.*, vol. 18, no. 3, pp. 1504–1517, Mar. 2019.

[34] X. Lin, J. Xia, and Z. Wang, "Probabilistic caching placement in UAV-assisted heterogeneous wireless networks," *Phys. Commun.*, vol. 33, pp. 54–61, Apr. 2019.

[35] D. Kim, J. Lee, and T. Q. S. Quek, "Performance analysis for multi-layer unmanned aerial vehicle networks," in *Proc. IEEE Globecom Workshops (GC Wkshps)*, Abu Dhabi, United Arab Emirates, Dec. 2018, pp. 1–6.

[36] C. Zhang and W. Zhang, "Spectrum sharing for drone networks," *IEEE J. Sel. Areas Commun.*, vol. 35, no. 1, pp. 136–144, Jan. 2017.

[37] J. G. Andrews, F. Baccelli, and R. K. Ganti, "A tractable approach to coverage and rate in cellular networks," *IEEE Trans. Commun.*, vol. 59, no. 11, pp. 3122–3134, Nov. 2011.

[38] X. Wang, H. Zhang, Y. Tian, and V. C. M. Leung, "Modeling and analysis of aerial base station-assisted cellular networks in finite areas under LoS and NLoS propagation," *IEEE Trans. Wireless Commun.*, vol. 17, no. 10, pp. 6985–7000, Oct. 2018.
[39] A. M. Hayajneh, S. A. R. Zaidi, D. C. McLernon, M. Di Renzo, and M. Ghogho, "Performance analysis of UAV enabled disaster recovery networks: A stochastic geometric framework based on cluster processes," *IEEE Access*, vol. 6, pp. 26215–26230, 2018.

CONGSHAN FAN received the B.S. degree from Nanchang University, China, in 2009, and the M.S. degree from the Beijing University of Posts and Telecommunications, China, in 2013, where she is currently pursuing the Ph.D. degree in information and communication engineering. Her current research interests include edge caching, UAVs networks, and ultra-dense networks.

TIANKUI ZHANG (M'10–SM'15) received the B.S. degree in communication engineering and the Ph.D. degree in information and communication engineering from the Beijing University of Posts and Telecommunications (BUPT), China, in 2003 and 2008, respectively. He is currently an Associate Professor with the School of Information and Communication Engineering, BUPT. He has published papers in conference such as the IEEE GLOBECOM and the IEEE ICC. His research interests include wireless communication networks, green wireless networks, signal processing for wireless communications, and content centric wireless networks. He has published more than 100 articles including journal articles on the IEEE JOURNAL ON SELECTED AREAS IN COMMUNICATIONS and the IEEE TRANSACTIONS ON COMMUNICATIONS.

ZHIMIN ZENG received the B.S. degree in carrier communication, the M.S. degree in communication and electronic systems, and the Ph.D. degree in communication and information systems from the Beijing University of Posts and Telecommunication, Beijing, China. He is currently a Professor with the School of Information and Communication Engineering, Beijing University of Posts and Telecommunications. He is a Senior Member of the China Institute of Communications, an Advanced Member of the Chinese Institute of Electronics, and a member of the Academic Committee, BUPT. His current research interest includes theory and technology of next generation mobile and wireless networks.